Photoluminescence Investigation Based on Laser Heating Effect in ZnO-Ordered Nanostructures

Yingling Yang,[†] Hongwei Yan,[†] Zhengping Fu,[†] Beifang Yang,*[,†] Linsheng Xia,[†] Yuandong Xu,[†] Jian Zuo,[‡] and Fanqing Li[‡]

Department of Materials Science and Engineering, University of Science and Technology of China, Hefei, Anhui 230026, P.R. China, and Structure Research Laboratory, University of Science and Technology of China, Hefei, Anhui 230026, P.R. China

Received: October 10, 2005; In Final Form: November 8, 2005

We synthesized ZnO−SiO_2 composite opal and ZnO inverse opal by electrodeposition using SiO_2−opal template and polystyrene (PS)−opal template, respectively. Compared with compact ZnO nanocrystal film also prepared by electrodeposition, ordered ZnO nanostructures exhibit more significant red-shift and broadening of the UV peak with increasing excitation power, which is due to a stronger local heating effect in ordered ZnO nanostructures. We developed a quantitative analytical method to investigate photoluminescence (PL) of ZnO based on laser heating effects. The experimental data agree well with fitting curves derived from the electron−phonon interaction model. Important parameters, such as electron−phonon coupling strength and thermal activation energy, can be obtained by fitting experimental data. The resonant Raman spectra provide further evidence that the analyses based on laser heating effects are feasible.

Introduction

There is an increasing interest in three-dimensional (3D) ordered nanostructures due to their growing applications in separations, sensors, catalysis, bioscience, and photonics.[1−11] Template methods using colloidal crystals such as silica and polystyrene (PS) provide a simple and effective route for fabricating 3D-ordered materials.[8−11] In the past few years, various types of ordered composite materials and ordered porous materials have been synthesized by using SiO_2−opal and PS−opal.[8,9,11] Although the fabrication of 3D-ordered materials has been widely explored, there is still a dearth of systematic investigation of optical properties of these materials.

Research on ZnO has generated great interest in recent years for its promising versatile applications, especially on short wavelength light-emitting, UV lasing, and transparent conducting materials, due to its wide direct gap of 3.37 eV and large exciton binding energy of 60 meV at room temperature.[12] Recently, several groups investigated optical properties of ZnO−opal composite materials and showed their good prospects for use in micro- and optoelectronics.[13−17] Ordered porous ZnO films are potential sensors and semiconducting electrodes by virtue of the large internal surface area and improved mass transportation.[18] Scharrer et al. have synthesized 3D-ordered porous ZnO by atomic layer deposition.[19] Electrochemical deposition, as a more convenient and cost-effective method, was used by Sumida et al. to obtain ZnO inverse opal.[18] Recently, by adding ethanol in the electrolyte to help wetting PS templates, we developed the electroplating technique in fabricating 3D-ordered macroporous ZnO.[20]

More recently, for wide band-gap semiconductor powder, Bergman et al. have confirmed that a large PL red-shift depending on excitation power is attributed to lasing heating and heat trapping.[21] Alim et al. have proved that even low-power ultraviolet laser excitation leads to strong local heating of the ZnO nanocrystals and causes a large red-shift of the optical phonon peaks in the resonant Raman spectra.[22−24] However, there is still no quantitative systematic investigation of the influence of laser heating effect on PL properties. Moreover, there are only reports of the PL red-shift of ZnO powder, which is not uniform and is unfit for quantitative investigation, thus further studies about red-shift, broadening, and excitation power dependence of luminescence from ZnO with uniform nanostructures are still necessary.

The purpose of this work is to investigate optical properties of ordered ZnO nanostructures. It was found that the UV PL band of ordered ZnO nanostructures exhibit more significant red-shift and broadening with increasing excitation power compared to that of compact ZnO nanocrystals film. We develop a quantitative analytical method to investigate the phenomenon based on laser heating effects. The experiment data agree well with fitting curves derived from the electron−phonon interaction model. We infer that a stronger local heating effect in ordered ZnO nanostructures results in the above phenomenon. Furthermore, we calculate the electron−phonon coupling strength determined by laser heating effect from PL spectra and find that it agrees with the result determined by the ratio of second- to first-order Raman scattering intensity from resonant Raman spectra, which provides further evidence for the feasibility of our analysis.

2. Experimental Section

Monodisperse SiO_2 spheres and PS spheres were prepared according to previous reports.[25] By using vertical deposition technique,[26] the PS− and SiO_2−opal films were obtained on indium tin oxide (ITO)-coated glass substrates. The electrochemical deposition was carried out by a potentiostatic technique in a three-electrode system by using a saturated calomel electrode (SCE) as the reference and Zn plates as counter

* To whom correspondence should be addressed. E-mail: bfyang@ustc.edu.cn.
[†] Department of Materials Science and Engineering.
[‡] Structure Research Laboratory.

10.1021/jp055757x CCC: $33.50
Published on Web 12/09/2005

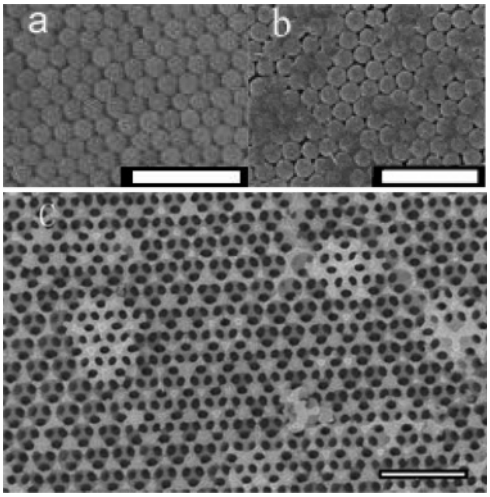

Figure 1. FESEM images. (a) Air−SiO_2 opal films. (b) ZnO−SiO_2 opal film. (c) ZnO inverse opal film. Scale bars represent 1 μm.

electrodes. ITO glasses (for compact ZnO nanocrystals film), SiO_2−opal/ITO (for ZnO−SiO_2 opal film), and PS−opal/ITO (for ZnO inverse opal film) were used as the substrate electrodes. The electrolytes were 0.04 M $Zn(NO_3)_2$ solutions, which were prepared by using water (for compact ZnO nanocrystals film and ZnO−SiO_2 opal film) or mixed ethanol−water solvents (for ZnO inverse opal film). The deposition temperature was kept at 62 °C, and the reference voltage was kept at −0.96 V vs SCE. To obtain ZnO inverse opal film, after electrodeposition, the samples were burned in air at 550 °C for 30 min to remove the PS templates.

Hereafter, we label compact ZnO nanocrystal film, ZnO−SiO_2 opal film, and ZnO inverse opal film as sample 1, sample 2, and sample 3, respectively.

The morphology was characterized by using a JSM-6700F field emission scanning electron microscope (FESEM). The X-ray diffraction (XRD) patterns were recorded on a Philips X'pert Prosuper diffractometer using Cu Kα irradiation (λ = 1.5419 Å). The transmittance measurement was carried out with a UV-2401 PC spectrophotometer. The PL and Raman measurement was carried out on a LABRAM-HR confocal laser micro-Raman spectrometer with a 325 nm He−Cd pump laser at room temperature. The laser beam was focused on the sample with a spot area of 20 μm^2 by a lens and the maximum excitation power was about 1 mW. The emitted signal from the sample was collected in a backscattering geometry configuration.

3. Results and Discussion

3.1. Structural and Spectroscopic Characterization. The air−SiO_2 opal films look uniformly blue when viewed with the naked eye in the direction normal to the sample surface. After filling with ZnO by cathodic electrodeposition, the resulting films turned to bright green, indicating a large-scale homogeneous filling process in the opal film. The colors of air−SiO_2 opal and ZnO−SiO_2 opal both show an angular dependence due to the angular dependence of an incomplete photonic stop band. The color change is caused by the increase of the average dielectric constant after deposition. Figure 1a is a typical FESEM surface image of the air−SiO_2 opal films, which reveals a well-ordered sphere array corresponding to the (111) surface of a face-centered cubic (fcc) structure. The FESEM surface image in Figure 1b shows that ZnO has been formed inside of the porous opal. The interspace of SiO_2−opal has been filled by ZnO. Because the growth rate of ZnO is not uniform inside the

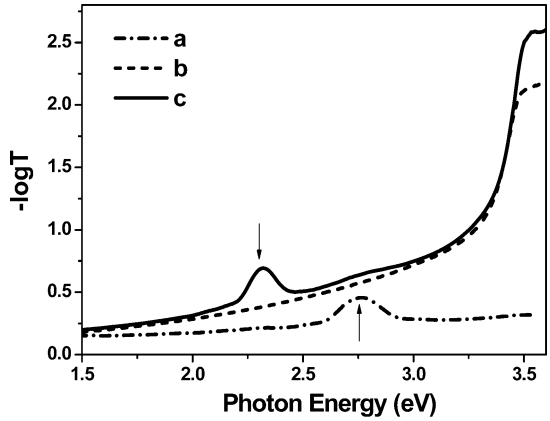

Figure 2. Optical transmission spectra of (a) air−SiO_2 opal film, (b) compact ZnO nanocrystals film, and (c) ZnO−SiO_2 opal films.

SiO_2−opal sample, in some zones, ZnO grows faster and reaches the upper surface, and in other zones, ZnO nanocrystals are still under the upper surface. Figure 1c shows SEM image of typical ordered macroporous ZnO film as viewed from the top. Holes into the layer below are clearly observed, indicating the 3D-ordered nature of the structures. The result suggests that there is no significant degradation of the structure after removal of PS template. Figure 2 shows the optical transmission spectra of air−SiO_2 opal film and ZnO−SiO_2 opal film. These spectra were collected in directions corresponding to $\theta = 0°$ with respect to the normal to the sample surface. A clear peak in the optical transmission of SiO_2−opal film can be observed due to Bragg reflection (*a* line). The *b* line is the transmission spectrum of ZnO−SiO_2 opal film, on which the redundant SiO_2 layers have been wiped away by alcohol-cotton before measurement. The Bragg reflection peak of this sample moves toward lower energies, as compared to that of air−SiO_2 opal film. By using Bragg's law for normal incidence, we estimated the ZnO filling fraction of the interstitial volume in SiO_2−opal to be ~95% by the red-shift of photonic stop band. Similar to the SiO_2−opal, the PS−opal also shows a color change after filling ZnO by electrodeposition. At last, the obtained ordered macroporous ZnO film showed uniform red. Details of the optical transmission spectra of ZnO inverse opal have been presented elsewhere.[20] The average sizes of ZnO nanocrystals in compact nanocrystal film and ZnO−SiO_2 opal film are about 35 nm and that in ZnO inverse opal film are about 28 nm, calculated by Scherrer equations.

3.2. Theory for Laser Heating Effects. Figure 3 shows the room-temperature PL spectra of compact ZnO nanocrystal film and ZnO−SiO_2 composite opal at different excitation powers. The photon energy of the UV peaks exhibits a significant red-shift with increasing excitation power. A broadening of the UV emission peak is also observed with increasing excitation power. According to the work of Bergman et al., the PL red-shift is attributed to lasing heating and heat trapping.[21] In fact, the laser energy is 3.815 eV and is strongly absorbed by ZnO nanocrystals of band gap ~3.3eV. In addition, the laser spot size is only ~5μm in diameter, thus the laser delivers a very high power density to the samples. Therefore, we consider that the lasing local heating is the dominant factor that leads to the PL red-shift and broadening in our samples. For a quantitative understanding of our results, we establish a simplified model to analyze the experimental data.

When a laser beam is focused on the surface of a sample, some of the optical energy is absorbed by ZnO nanocrystals, causing a radiative transition process and a nonradiative transition process. Only the optical energy causing a nonradiative

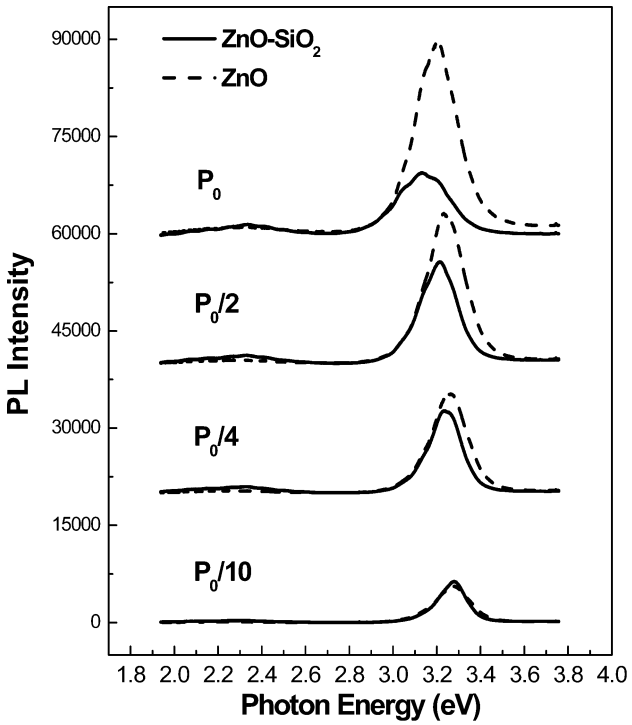

Figure 3. PL spectra of ZnO nanocrystals film and ZnO−SiO_2 composite opal at the different excitation powers.

transition process is transformed into heat energy. Therefore, the power density of heat (P_h) can be expressed as

$$P_h = K(1 - \Phi)FP \tag{1}$$

where Φ is the total luminescence quantum yield when the sample is being irradiated with an excitation power of P. F is the fraction of incident light absorbed by ZnO nanocrystals, and K is a proportionality constant. The laser heats the ZnO nanocrystals, and then the heat is being transferred from the heating area into the environment. When the heat flow is steady, there is a relation between the power density of heat (P_h) and the temperature at the heating area (T):

$$P_h \approx \lambda(T - T_0) \tag{2}$$

where λ is the coefficient, and $T_0 = 283$ K is the ambient temperature. According to eqs 1 and 2, the following equation could be deduced:

$$K(1 - \Phi)FP \approx \lambda(T - T_0) \Rightarrow T \approx \mu P + T_0 \tag{3}$$

where μ is a coefficient, and $\mu = (K(1 - \Phi)F)/\lambda$. Under the same excitation power, a larger μ should lead to a stronger local heating effect.

Previously, it has been proved that the temperature dependence of the interband transition energies can be described by a Bose−Einstein-type expression.[21,27]

$$E(T) = E(0) - 2a_B/[\exp(\Theta_B/T) - 1] \tag{4}$$

This relation represents the modification of a band gap of a semiconductor due to the electron−phonon interaction. In eq 4, $E(0)$ is the transition energy at 0 K, a_B represents the strength of the exciton−average phonon interaction, and Θ_B corresponds to the average phonon temperature. It has been shown that the temperature of ZnO can go to several hundred degrees Celsius by laser heating, even at a low excitation.[21−24] The higher the temperature is, the lower Θ_B/T is. Therefore, we do a Taylor series approximation to $\exp(\Theta_B/T)$

$$\exp(\Theta_B/T) \approx 1 + \frac{\Theta_B}{T} + \frac{1}{2}\left(\frac{\Theta_B}{T}\right)^2 + \cdots\cdots \tag{5}$$

We neglect the terms of order higher than first in the expression (eq 5), and obtain the following equation from eq 4:

$$E(T) \approx E(0) - \alpha T \tag{6}$$

where $\alpha = 2a_B/\Theta_B$. The interband transition energy is monotonically decreasing with the temperature. This phenomenon has been observed by Bagnall et al. from ZnO epitaxial layers[28] when the temperature is higher than room temperature. By plugging eq 3 into eq 6, we get the following expression:

$$E(P) \approx E(0) - \alpha T_0 - \alpha\mu P \tag{7}$$

There is a linear relation between the interband transition energy ($E(P)$) and the excitation power of the laser (P).

The temperature dependence of the line width of the interband transitions of semiconductors can be expressed as[27]

$$\Gamma(T) = \Gamma(0) + \Gamma_{ep}/[\exp(\Theta_{LO}/T) - 1] \tag{8}$$

where $\Gamma(0)$ represents the broadening from temperature-independent mechanisms, such as impurity, dislocation, and surface scattering, and electron−electron interaction, whereas the second term is caused by the exciton−LO-phonon (Fröhlich) interaction. The quantity Γ_{ep} represents the strength of the exciton−LO-phonon coupling, while Θ_{LO} is the LO-phonon temperature. By taking eq 3 in eq 8, we arrive at the following expression:

$$\Gamma(P) = \Gamma(0) + \Gamma_{ep}/[\exp(\Theta_{LO}/(\mu P + T_0) - 1] \tag{9}$$

This equation describes the relation between the line width of the interband transitions and the excitation power. By considering $\hbar\omega_{LO} \approx 71$ (meV) by Raman spectra and $\Theta_{LO} = \omega_{LO}\hbar/k_B$, where k_B is Boltzman constant, we obtain $\Theta_{LO} \approx 823$ K.

It has been proved that the intensity O of the spontaneous free-exciton emission band grows linearly with the excitation intensity I for bulk ZnO.[29] In the same irradiated area, the excitation power $P \propto I$. Therefore, for the bulk ZnO,

$$O \propto P \tag{10}$$

The temperature dependence of the integrated PL intensity can be expressed by the equation.[30]

$$O = O_0[1 + D\exp(-E_x/k_BT)]^{-1} \tag{11}$$

where E_x is the activation energy, and O_0 and D are constants. According to expressions 10 and 11, considering the laser heating effect, we assume that the expression of the UV-integrated intensity of the ZnO nanostructure is

$$O = \xi_0 P[1 + D\exp(-E_x/k_BT)]^{-1} \tag{12}$$

where ξ_0 is a constant. By combining eqs 3 and 12, we get the following expression:

$$O(P) = \xi_0 P\{1 + D\exp[-E_x/k_B(\mu P + T_0)]\}^{-1} \tag{13}$$

Equation 13 describes the relation between the UV-integrated intensity of ZnO nanocrystals and the excitation power.

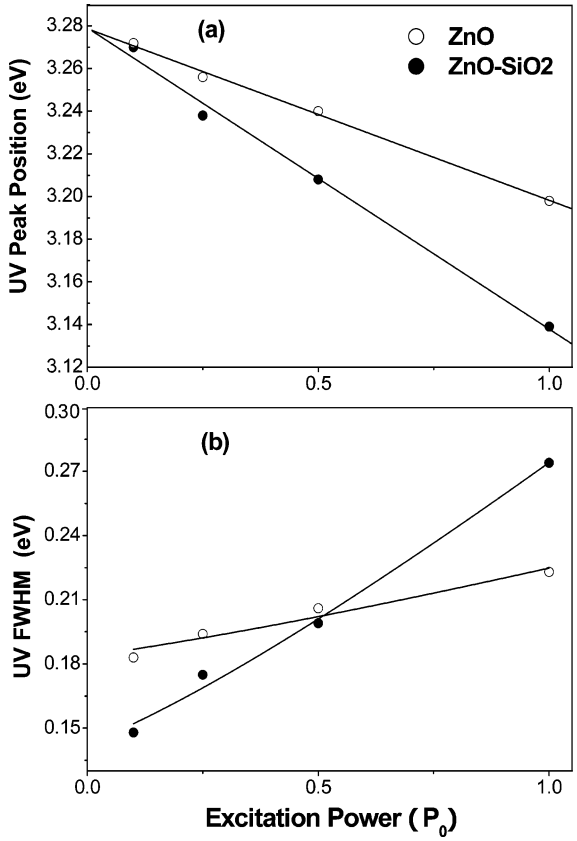

Figure 4. (a) PL energies of ZnO nanocrystals film and ZnO−SiO_2 composite opal as a function of excitation power. (b) UV fwhm of compact ZnO film and ZnO−SiO_2 composite opal as a function of excitation power. The fitting curve is shown as a solid line.

3.3. PL Analysis for ZnO Nanocrystals Film and ZnO−SiO_2 Composite Opal. A strong UV emission was observed in the PL spectra of compact ZnO nanocrystals film and ZnO−SiO_2 composite opal (Figure 3), which should be a near-band-edge emission of ZnO nanocrystals due to exciton-related activity. The visible emission, which is ascribed to a deep-level defect emission, is relatively low. The UV PL intensity of compact ZnO film is monotonically increasing with the excitation power. However, the UV PL intensity of the ZnO−SiO_2 composite opal is abnormal. It increases in the region 0.1−0.5 P_0, reaches its highest intensity at 0.5 P_0, and decreases at 1P_0. A similar phenomenon has been observed by Bergman et al. that the PL intensity at higher laser power is reduced other than saturated in a general case.[21] They considered that heat damage to the powder results in the behavior of PL. However, we infer that the behavior is due to heat quenching of luminescence because of the prediction of the UV-integrated intensity as a function of power given by eq 13. It was observed that the UV energy of ZnO−SiO_2 composite opal shows a larger red-shift with increasing excitation power than that of compact ZnO film. Compared with the compact ZnO film, a more significant broadening of the UV emission peak is also observed in the ZnO−SiO_2 composite opal.

The PL energies of compact nanocrystals ZnO film and ZnO−SiO_2 composite opal as a function of excitation power are presented in Figure 4a. Equation 7 successfully describes the excitation power dependence of the UV peak position. The fitting curve from eq 7 is shown as a solid line through the data points in Figure 4a. By taking $E(0) = 3.377$eV from ref 31 and fitting the experimental data, we obtained the following results: $\alpha_1 \approx 3.46 \times 10^{-4}$ (eV/K), $\mu_1 P_0 \approx 2.31 \times 10^2$ K, $\alpha_2 \approx 3.46 \times 10^{-4}$ (eV/K) and $\mu_2 P_0 \approx 4.08 \times 10^2$ K. The subscript numbers indicate the samples. The full width at half-maximum (fwhm) of compact ZnO film and ZnO−SiO_2 composite opal as a function of excitation power are presented in Figure 4b. This expression (eq 9) can give an adequate prediction of the fwhm of the UV peaks as a function of power. By fitting the data, we obtained $\Gamma_{ep1} \approx 0.21$(eV) and $\Gamma_{ep2} \approx 0.35$(eV). The UV intensity of ZnO nanocrystal film and ZnO−SiO_2 composite opal as a function of excitation power are presented in Figure 5. By using eq 13 to fit the experiment data, we obtained $E_1 \approx 0.12$ (eV) and $E_2 \approx 0.20$ (eV).

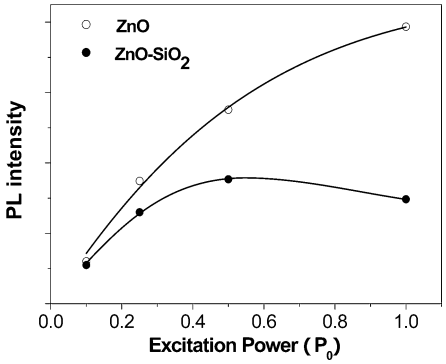

Figure 5. UV intensity of ZnO nanocrystals film and ZnO−SiO_2 composite opal as a function of excitation power. The fitting curve is shown as a solid line.

3.4. PL Analysis for Ordered Macroporous ZnO. To confirm our above analysis method, we further investigated the UV emission of ordered macroporous ZnO. The fabricating condition and structure of macroporous ZnO is different from those of ZnO nanocrystals film and ZnO−SiO_2 composite opal. Therefore, if our above equations agree with the data of ZnO inverse opal, it means our analysis method is universal for wide band-gap semiconductor nanostructure materials.

Figure 6 shows the room-temperature PL spectra of ordered macroporous ZnO film at the different excitation powers. Similar to the above two samples, the photon energy of the UV peak exhibits a significant red-shift with increasing excitation power. There is a good linear relation between the UV peak position and excitation power (Figure 7a). By using eq 7 to fit the experiment data, we obtained $\alpha_3 \approx 4.49 \times 10^{-4}$ (eV/K) and $\mu_3 P_0 \approx 3.85 \times 10^2$ K. Figure 7b show the UV fwhm of macroporous ZnO film as a function of excitation power. A broadening of the UV emission peak is also observed. The fitting curve from eq 9 is shown as a solid line through the data points. It is found that the theory curve agrees well with the experimental data. By fitting the data, we obtained $\Gamma_{ep3} \approx 0.28$ (eV). The UV intensity of ordered macroporous ZnO film as a function of excitation power is presented in Figure 8. The theory curve agrees well with the experimental data, and we obtained $E_3 \approx 0.30$(eV).

3.5. Further Discussions. Under the same excitation power, a larger μ should lead to a stronger local heating effect. It can be found that there is a stronger local heating effect in ZnO-nanostructured films ($\mu_2 P_0 \approx 4.08 \times 10^2$ K and $\mu_3 P_0 \approx 3.85 \times 10^2$ K) than in compact ZnO film ($\mu_1 P_0 \approx 2.31 \times 10^2$ K). The stronger local heating effect induces a larger red-shift and broadening of the UV emission peak. It also leads to a slower increase of the UV intensity with an increase of the excitation power. The origins of the stronger local heating effect for ZnO-nanostructured films may be: (1) Heat is trapped and convective cooling becomes more inefficient due to the convoluted geometry of ordered nanostructures.[21] (2) There is a large

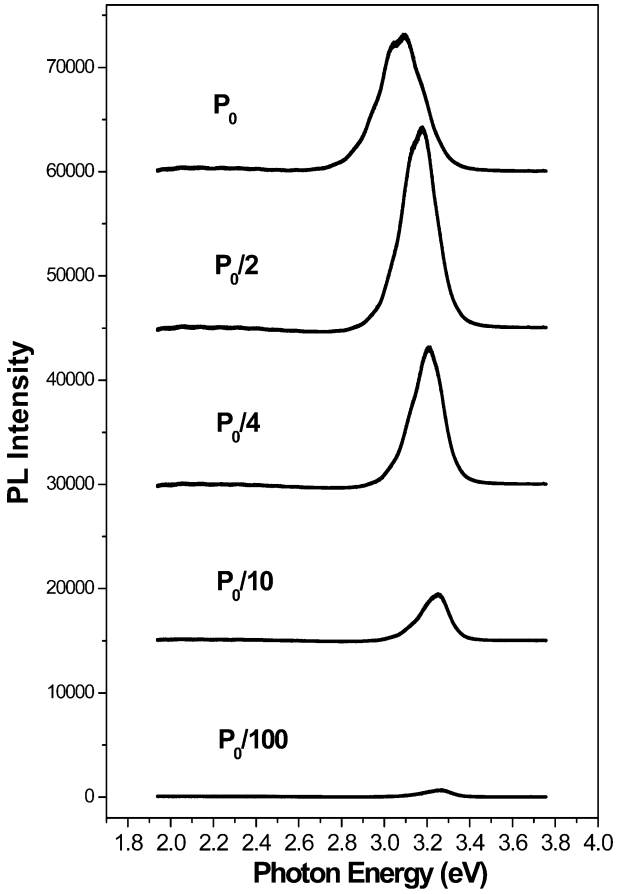

Figure 6. PL spectra of ordered macroporous ZnO film at the different excitation powers.

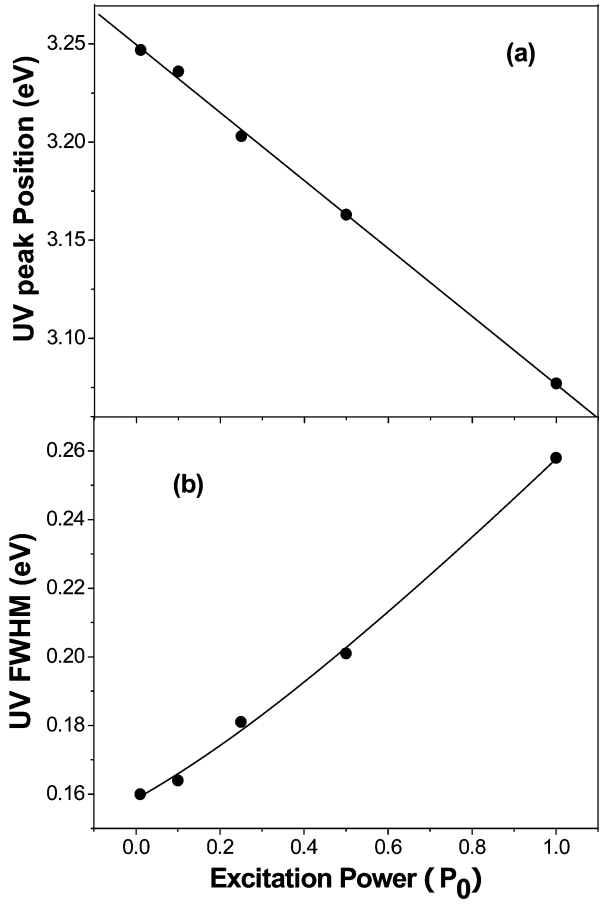

Figure 7. (a) PL energies of ordered macroporous ZnO as a function of excitation power. (b) UV fwhm of ordered macroporous ZnO as a function of excitation power. The fitting curve is shown as a solid line.

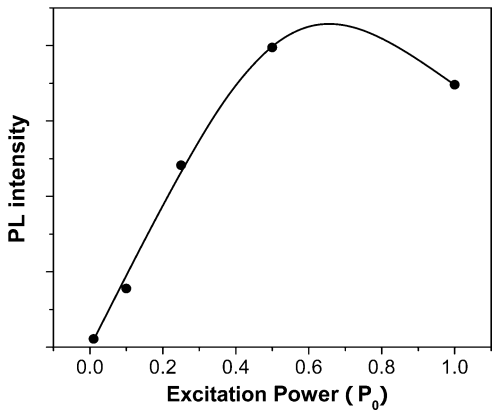

Figure 8. UV intensity of ordered macroporous ZnO as a function of excitation power. The fitting curve is shown as solid line.

amount of air in the pores of ZnO inverse opal, and SiO_2 spheres in ZnO−SiO_2 opal. As a result, the thermal conductivity of ZnO films with ordered nanostructures is drastically reduced. It is noticeable that the thermal conductivity of macroporous ZnO is lower than that of ZnO−SiO_2 composite opal because of extremely low thermal conductivity of air, but the laser heating effect of it is smaller than that of ZnO−SiO_2 composite opal. The explanation for this phenomenon is that the laser heating effect is determined by both thermal conductivity and probability of nonradiative recombination ($\mu = (K(1 - \Phi)F)/\lambda$). Macroporous ZnO exhibits stronger UV emission and better crystalline quality due to the process of removing the template through which ZnO−PS composites are calcined in air at 550 °C. Therefore, although the thermal conductivity of macroporous ZnO is lower, it does not show a stronger heating effect because of a lower probability of nonradiative recombination. A supplemental experiment was adopted in which ordered macroporous ZnO was prepared by dissolving a PS template in toluene at room temperature. This avoided annealing treatment and preserved nonradiative recombination centers. The PL measurements show that there is a stronger laser heating effect in this material ($\mu P \approx 4.21 \times 10^2$ K) than that in ZnO−SiO_2 composite opal.

We measured the Raman spectra of the above three samples at the same excitation power (Figure 9). In our measurement range, the Raman spectra are dominated by the peak at about 575 cm^{-1}. The 575 cm^{-1} Raman peak was ascribed by some authors as being due to either the LO phonon of A_1 or the LO phonon of E_1.[22] The line shapes of 575 cm^{-1} peak is asymmetric in ZnO−SiO_2 composite opal and macroporous ZnO. A detailed fitting of this broad peak reveals two components located at 575 and 550 cm^{-1}. The low-frequency peak may be the interface−phonon mode according to the peak position.[32] In principle, the strength of the exciton−LO-phonon coupling can be probed by Raman scattering experiments directly because the ratio between the second- and first-order scattering cross section $I_{(2LO)}/I_{(LO)}$ is a very sensitive function of the electron−LO-phonon coupling strength.[33] By introducing the integrated intensities of Raman peaks in expression $I_{(2LO)}/I_{(LO)}$, we obtained the ratios of our samples, which are presented in the table inserted in Figure 10. Figure 10 shows the values of $I_{(2LO)}/I_{(LO)}$, which are plotted as function of the exciton−LO-phonon coupling strength (Γ_{ep}) that were obtained by fitting the fwhm of the UV emission band. The intensity ratio increases with increasing Γ_{ep}. There is an approximate linear relation between $I_{(2LO)}/I_{(LO)}$ and Γ_{ep}. The data obtained from fitting curves based on laser heating effects agree with the data obtained from Raman

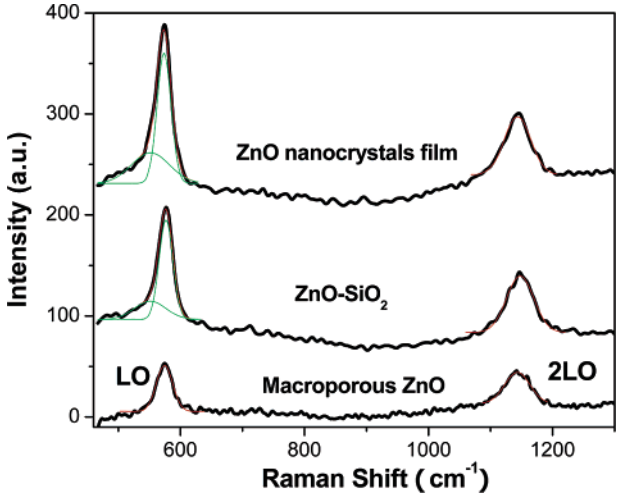

Figure 9. Raman spectra of samples at the same excitation power. The black line is the experimental result, and the color lines are Lorentzian fit for Raman peaks.

Sample	Compact ZnO	Macroporous ZnO	ZnO/SiO_2
Γ_{ep} (10^2meV)	2.1	2.8	3.5
$I_{(2LO)}/I_{(LO)}$	0.84	1.0	1.1

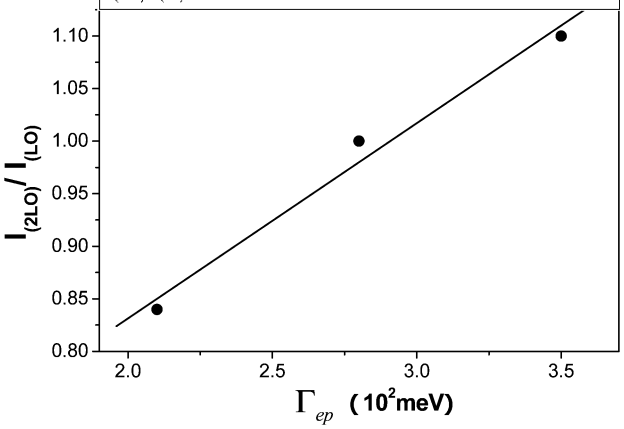

Figure 10. The values of $I_{(2LO)}/I_{(LO)}$ as a function of the exciton−LO-phonon coupling strength (Γ_{ep}) that are obtained by fitting the fwhm of the UV emission band.

scattering spectra, which is additional evidence that the analyses of ZnO UV emission based on laser heating effects is feasible.

The constant α represents the temperature dependence of the UV emission peak of ZnO at a high temperature range. The values of α determined by the laser heating effect from PL spectra in this paper are similar to the values obtained by temperature-varying PL measurements in previous studies.[34−36] However, the exciton−LO-phonon coupling strength (Γ_{ep}) of our samples were significantly smaller than 0.8761 eV in bulk ZnO.[37] It has been observed in ZnO nanowires,[33] ZnO nanocrystals,[36] and ZnO/ZnMgO multiquantum wells[38] that Γ_{ep} is largely reduced compared with that of bulk ZnO. Wang et al. considered the following two factors causing the decrease of Γ_{ep} of nanometer-scale ZnO materials.[33] (1) The momentum conservation rule is relaxed for nanocrystals. (2) The quantum confinement strongly modifies the eigenfunctions and causes the change of the exciton radius and dielectric coefficient and, finally, has profound consequences on the magnitude of the coupling.

The thermal activation energy is usually close to the binding energy of the free exciton in ZnO films.[31] From the fitting result, the thermal activation energy $E_1 \approx 0.12$ (eV), $E_2 \approx 0.20$ (eV), and $E_3 \approx 0.30$ (eV), which are larger than that of bulk ZnO (0.060 eV). The value of E_1 is close to the thermal activation energy of ZnO nanocrystals films prepared on Si (100) substrates by the sol−gel process.[31] The possible reason for the enhancement of activation energy in compact ZnO nanocrystals film is that the grain sizes of ZnO are much larger than the Bohr radius and smaller than the excitonic coherent wavelength, thus the binding energy of the free excition is enhanced because of the increasing oscillator strengths.[28,31] The thermal activation energies of ZnO films with ordered nanostructures are even larger than that of compact ZnO nanocrystals film. We are confused about such large activation energies in ZnO ordered nanostructures. Recently, Chen et al. observed an intensive UV emission from ZnO nanosheets, even at 857 K, and they considered that it is due to the large increase of exciton binding energy.[39] It is possible that such large activation energies are the only apparent parameters arising from the complex radiative recombination kinetics of ZnO at high temperature. Considering that the temperature is high in ZnO-ordered structures at high excitation power ($T \approx \mu P + T_0$, thus $T_2 \approx 691$ K and $T_3 \approx 618$ K at P_0), thermal fluctuation $\sim K_B T$ is comparable with the recognized exciton binding energy (0.060 eV), thus free carrier concentration is large due to ionization of excitons. The contribution arising from free carrier recombination is not negligible. It has been proved in GaAs/AlGaAs quantum well structures that free excitons coexist with electrons and holes coming from excition dissociation at high temperature, and the ratio of the populations of free carriers to free excitons increases with temperature increase.[40] Therefore, there is a larger intensity difference between the overall PL and excition PL.[40] We assumed that the overall UV emission intensity is exciton PL intensity in quantitative analyses process, which may be responsible for the large specious activation energy. Up to now, there are few investigations on high-temperature PL characteristics of ZnO, and it is difficult to understand the radiative recombination kinetics at high temperature. To clarify the phenomenon, more studies are needed in the future.

4. Conclusions

In conclusion, we successfully synthesized ZnO−SiO_2 composite opal and ZnO inverse opal by electrodeposition using SiO_2−opal template and PS−opal template, respectively. The UV PL peak of ZnO films with ordered nanostructures exhibit more significant red-shift and broadening than that of compact ZnO nanocrystal film with increasing excitation power, which is due to the stronger local heating effect in ordered ZnO nanostructures. A simple model based on laser heating effects is used to analyze UV PL of ZnO films, which agrees well with the experiment data. It was found that the electron−phonon coupling strengths determined by the ratio of second- to first-order Raman scattering cross sections from the resonant Raman spectra agree with that determined by laser heating effects from PL spectra, which provides further evidence that our analyses are feasible.

Acknowledgment. This work is supported by China National Natural Science Research Foundation.

References and Notes

(1) Stein, A.; Schroden, R. C. *Curr. Opin. Solid State Mater. Sci.* **2001**, *5*, 553.

(2) Lee, K.; Asher, S. A. *J. Am. Chem. Soc.* **2000**, *122*, 9534.

(3) Holtz, J. H.; Asher, S. A. *Nature* **1997**, *389*, 829.

(4) Asher, S. A.; Alexeev, V. L.; Goponenko, A. V.; Sharma, A. C.; Lednev, I. K.; Wilcox, C. S.; Finegold, D. N. *J. Am. Chem. Soc.* **2003**, *125*, 3322.

(5) Sharma, A. C.; Jana, T.; Kesavamoorthy, R.; Shi, L. J.; Virji, M. A.; Finegold, D. N.; Asher, S. A. *J. Am. Chem. Soc.* **2004**, *126*, 2971.

(6) Nishimura, S.; Abrams, N.; Lewis, B. A.; Halaoui, L. I.; Mallouk, T. E.; Benkstein, K. D.; van de Lagemaat, J.; Frank, A. J. *J. Am. Chem. Soc.* **2003**, *125*, 6306.

(7) Weissman, J. M.; Sunkara, H. B.; Tse, A. S.; Asher, S. A. *Science* **1996**, *274*, 959.

(8) Lopez, C. *Adv. Mater.* **2003**, *15*, 1679.

(9) Jiang, P.; McFarland, M. J. *J. Am. Chem. Soc.* **2004**, *126*, 13778.

(10) Wong, S.; Kitaev, V.; Ozin, G. A. *J. Am. Chem. Soc.* **2003**, *125*, 15589.

(11) Xia, Y. N.; Gates, B.; Yin, Y. D.; Lu, Y. *Adv. Mater.* **2000**, *12*, 693.

(12) Tang, Z. K.; Wong, G. K. L.; Yu, P.; Kawasaki, M.; Ohtomo, A.; Koinuma, H.; Segawa, Y. *Appl. Phys. Lett.* **1998**, *72*, 3270.

(13) Ursaki, V. V.; Tiginyanu, I. M.; Zalamai, V. V.; Masalov, V. M.; Samarov, E. N.; Emelchenko, G. A.; Briones, F. *J. Appl. Phys.* **2004**, *96*, 1001.

(14) Gruzintsev, A.; Volkov, V.; Emelchenko, G. A.; Karpov, I. A.; Maslov, W. M.; Michailov, G. M.; Yakimov, E. E. *Thin Solid Films* **2004**, *459*, 111.

(15) Ursaki, V. V.; Tiginyanu, I. M.; Zalamai, V. V.; Rusu, E. V.; Emelchenko, G. A.; Masalov, V. M.; Samarov, E. N. *Phys. Rev. B* **2004**, *70*, 155204.

(16) Abrarov, S. M.; Yuldashev, S. U.; Lee, S. B.; Kang, T. W. *J. Lumin.* **2004**, *109*, 25.

(17) Yang, Y. L.; Yang, B. F.; Fu, Z. P.; Yan, H. W.; Wang, Z.; Dong, W. W.; Xia, L. S.; Liu, W. Q.; Zuo, J.; Li, F. Q. *J. Phys.: Condens. Matter* **2004**, *16*, 7277.

(18) Sumida, T.; Wada, Y.; Kitamura, T.; Yanagida, S. *Chem. Lett.* **2001**, 38.

(19) Scharrer, M.; Wu, X.; Yamilov, A.; Cao, H.; Chang, R. P. H. *Appl. Phys. Lett.* **2005**, *86*, 151113.

(20) Yan, H. W.; Yang, Y. L.; Fu, Z. P.; Yang, B. F.; Xia, L. S.; Fu, S. Q.; Li, F. Q. *Electrochem. Commun.* **2005**, *7*, 1122.

(21) Bergman, L.; Chen, X. B.; Morrison, J. L.; Huso, J.; Purdy, A. P. *J. Appl. Phys.* **2004**, *96*, 675.

(22) Alim, K. A.; Fonoberov, V. A.; Shamsa, M.; Balandin, A. A. *J. Appl. Phys.* **2005**, *97*, 124313.

(23) Alim, K. A.; Fonoberov, V. A.; Balandin, A. A. *Appl. Phys. Lett.* **2005**, *86*, 053103.

(24) Chen, X. B.; Morrison, J. L.; Huso, J.; Bergman, L.; Purdy, A. P. *J. Appl. Phys.* **2005**, *97*, 024302.

(25) Stober, W.; Fink, A.; Bohn, E. *J. Colloid Interface Sci.* **1968**, *26*, 62. Holland, B. T.; Blanford, C. F.; Do, T.; Stein, A. *Chem. Mater.* **1999**, *11*, 795.

(26) Jiang, P.; Bertone, J. F.; Hwang, K. S.; Colvin, V. L. *Chem. Mater.* **1999**, *11*, 2132. Kuai, S. L.; Hu, X. F.; Hache, A.; Truong, V. V. *J. Cryst. Growth* **2004**, *267*, 317.

(27) Li, C. F.; Huang, Y. S.; Malikova, L.; Pollak, F. H. *Phys. Rev. B* **1997**, *55*, 9251.

(28) Bagnall, D. M.; Chen, Y. F.; Zhu, Z.; Yao, T.; Shen, M. Y.; Goto, T. *Appl. Phys. Lett.* **1998**, *73*, 1038.

(29) Guo, B.; Qiu, Z. R.; Wong, K. S. *Appl. Phys. Lett.* **2003**, *82*, 2290.

(30) Jiang, D. S.; Jung, H.; Ploog, K. *J. Appl. Phys.* **1988**, *64*, 1371.

(31) Zhang, Y.; Lin, B. X.; Sun, X. K.; Fu, Z. X. *Appl. Phys. Lett.* **2005**, *86*, 131910.

(32) Fonoberov, V. A.; Balandin, A. A. *Phys. Rev. B* **2004**, *70*, 233205.

(33) Wang, R. P.; Xu, G.; Jin, P. *Phys. Rev. B* **2004**, *69*, 113303.

(34) Hur, T. B.; Jeen, G. S.; Hwang, Y. H.; Kim, H. K. *J. Appl. Phys.* **2003**, *94*, 5787.

(35) Youn, C. J.; Jeong, T. S.; Han, M. S.; Kim, J. H. *J. Cryst. Growth* **2004**, *261*, 526.

(36) Zhang, X. T.; Liu, Y. C.; Zhi, Z. Z.; Zhang, J. Y.; Lu, Y. M.; Shen, D. Z.; Xu, W.; Zhong, G. Z.; Fan, X. W.; Kong, X. G. *J. Phys. D: Appl. Phys.* **2001**, *34*, 3430.

(37) Makino, T.; Chia, C. H.; Tuan, N. T.; Segawa, Y.; Kawasaki, M.; Ohtomo, A.; Tamura, K.; Koinuma, H. *Appl. Phys. Lett.* **2000**, *76*, 3549.

(38) Sun, H. D.; Makino, T.; Tuan, N. T.; Segawa, Y.; Kawasaki, M.; Ohtomo, A.; Tamura, K.; Koinuma, H. *Appl. Phys. Lett.* **2001**, *78*, 2464.

(39) Chen, S. J.; Liu, Y. C.; Shao, C. L.; Mu, R.; Lu, Y. M.; Zhang, J. Y.; Shen, D. Z.; Fan, X. W. *Adv. Mater.* **2005**, *17*, 586.

(40) Colocci, M.; Curioli, M.; Vinattieri, A. *J. Appl. Phys.* **1990**, *68*, 2809.